ROYAL SOCIETY
OF CHEMISTRY

EDGE ARTICLE

Check for updates

Eight-electron copper-hydride nanoclusters: synthesis, structure, alloying chemistry and photoluminescence†

Jing Sun,‡[a] Jiahe Liu,‡[b] Hai-Feng Su,‡[c] Simin Li,[a] Xiongkai Tang,[c] Zhenlang Xie, [d] Zhen Xu,[c] Wenya Jiang,[e] Jianyu Wei, [e] Xuekun Gong,[a] Ayisha He,[a] Song Wang,*[b] De-en Jiang, [f] Nanfeng Zheng *[cg] and Hui Shen *[a]

The first copper-hydride nanocluster featuring eight free valence electrons has been successfully isolated and characterized spectroscopically. The structure of the nanocluster, represented by the chemical formula $[Cu_{47}(PhSe)_{15}(PPh_3)_5(CF_3COO)_{12}H_{12}]$ (referred to as $Cu_{47}H_{12}$, where PPh_3 denotes triphenylphosphine), has been precisely determined through single crystal X-ray diffraction analysis. Several distinguishing features differentiate the $Cu_{47}H_{12}$ clusters from previously reported examples. In terms of composition, these clusters represent a rare instance of high-nuclearity Cu nanoclusters containing hydride and stabilized by selenolate ligands. From an electronic standpoint, the stabilization of the nanocluster is achieved through its eight free valence electrons, marking it as the first copper-hydride cluster with this configuration. The alloying chemistry of the nanocluster also introduces unexpected findings in the field. The incorporation of silver atoms leads to the formation of $[(CuAg)_{47}(PhSe)_{18}(PPh_3)_6(CF_3COO)_{12}H_6]^{3+}$ clusters, which exhibit significant structural differences from the parent cluster. Both the homo and alloy clusters display dual-emission properties at 298 K, with the clusters additionally showcasing triple or even quadruple emission at 77 K. This work is anticipated to stimulate research interest in hydride-containing metal nanoclusters, focusing not only on compositional tailoring and structural engineering, but also on electronic structure details and potential applications.

[a]College of Energy Materials and Chemistry, Inner Mongolia University, Hohhot 010021, China. E-mail: shen@imu.edu.cn

[b]Key Laboratory of Precision and Intelligent Chemistry, School of Chemistry and Materials Science, University of Science and Technology of China, Hefei, Anhui 230026, China. E-mail: wsong09@ustc.edu.cn

[c]New Cornerstone Science Laboratory, State Key Laboratory for Physical Chemistry of Solid Surfaces, Collaborative Innovation Center of Chemistry for Energy Materials, National & Local Joint Engineering Research Center of Preparation Technology of Nanomaterials, College of Chemistry and Chemical Engineering, Xiamen University, Xiamen 361005, China. E-mail: nfzheng@xmu.edu.cn

[d]College of Food Science and Engineering, Guangdong Ocean University, Yangjiang 529500, China

[e]School of Materials and New Energy, Ningxia University, Yinchuan, Ningxia 750021, China

[f]Department of Chemical and Biomolecular Engineering, Vanderbilt University, Nashville, Tennessee 37235, USA

[g]Innovation Laboratory for Sciences and Technologies of Energy Materials of Fujian Province (IKKEM), Xiamen 361102, China

† Electronic supplementary information (ESI) available. CCDC 2376750 and 2258390. For ESI and crystallographic data in CIF or other electronic format see DOI: https://doi.org/10.1039/d4sc08547g

‡ These authors contributed equally to this work.

1 Introduction

Ligand-protected coinage metal nanoclusters (NCs) with precise molecular compositions and exact structural characteristics have garnered significant attention in fundamental research.[1–6] These nanomaterials are widely applicable in various fields, including catalysis, sensing, biology, and electronics, and they serve as model systems for gaining atomistic insights into the structure-and-property relationships of nanoscale/microscale materials.[7–19] Among metal NCs, those stabilized by hydrides are of particular interest due to their crucial roles in both the formation and stabilization of unique nanostructures, as well as in the functionalization of metal NCs to facilitate their applications.[20–23] In recent years, there has been a growing body of literature on metal-hydride NCs, encompassing metals ranging from copper, silver, gold to alloys.[24–28] These studies have explored a variety of ligands including phosphines, thiolates, alkynyls, and carbenes, highlighting promising applications in transformations, hydrogen evolution and catalysis.[29–34] For instance, through systematic investigation using neutron diffraction, Liu and colleagues have systematically demonstrated the coordination modes of hydride inside the metal framework in a family of hydride-containing copper and silver

metal NCs.[35–37] Additionally, research groups led by Tsukuda, Crudden, and Wang have revealed that gold-hydride NCs serve as key intermediates for further transformation into metallic NCs or efficient catalysts in the reduction of unsaturated compounds such as ketones, alkynes, and CO_2.[38–42]

Despite the significant progress, several fundamental issues regarding hydride-rich metal nanoclusters (NCs) remain: (1) in terms of synthesis, while efficient strategies are available for copper-hydride NCs, and recently a few silver variants, achieving high-nuclearity hydride-doped Cu NCs has proven more challenging.[43–45] (2) Metal-hydride NCs are typically considered metastable, making the attainment of hydride-rich metal NCs with a high number of free valence electrons quite challenging.[46–48] To the best of our knowledge, the existence of eight electron copper-hydride NCs has not been experimentally validated thus far.[49,50] (3) Although alloying strategies have been frequently employed to tailor the composition, electronic structure and properties of hydride-free NCs, wherein the structural integrity of parent clusters often remains intact, the alloying chemistry of copper-hydride nanoclusters is poorly understood.[51–53] In this scenario, there is a strong desire to expand the existing collection of copper-hydride nanoclusters in order to gain a comprehensive understanding of their various synthetic methods, bonding and electronic structures, and even the relationships between structure and property.

In this study, we present the synthesis, structural determination, electronic structure analysis, and alloying chemistry of a novel cluster known as $[Cu_{47}(PhSe)_{15}(PPh_3)_5(CF_3COO)_{12}H_{12}]$ (referred to as $Cu_{47}H_{12}$ hereafter). This nanocluster is the first eight-electron copper nanocluster to incorporate hydrides. Its one-pot and high-yield synthesis involving the reduction of copper salts in the presence of selenolate ligands allows for comprehensive characterization of its composition, purity, structure, and electronic properties. Notably, the alloying of external silver ions into the cluster results in the formation of a new group of clusters, $[(CuAg)_{47}(PhSe)_{18}(PPh_3)_6(CF_3COO)_{12}H_6]^{3+}$ ($(CuAg)_{47}H_6$), which exhibits a completely novel molecular structure. Both clusters are distinguished by their dual, triple, or even quadruple-emission photoluminescent properties.

2 Results and discussion

2.1 Synthesis and atomic structure

The absence of copper-hydride NCs with eight electrons in the literature underscores the challenges associated with effectively stabilizing Cu(0)-containing copper-hydride NCs. On one hand, the much lower half-cell reduction potential of copper (0.52 V) compared to silver (0.80 V) and gold (1.69 V) makes the Cu(0)-containing clusters highly sensitive to air, making their synthesis difficult.[47,49] On the other hand, the reactive nature of hydride atoms within these structures complicates the isolation of copper-hydride NCs.[26,54] To address these challenges, our strategy is to use bis(triphenylphosphine)copper tetrahydroborate ($(PPh_3)_2CuBH_4$) as the reducing agent in the synthesis.[54,55] This reductant not only provides the necessary hydride atoms for reduction and stabilization but also acts as

a carrier for surface ligands.[56,57] The $Cu_{47}H_{12}$ clusters were prepared by reducing a mixture of $Cu(CF_3COO)_2$ and PhSeH ligands using $(PPh_3)_2CuBH_4$ as the reductant (further details can be found in the ESI†). It is important to note that the one-pot synthetic prototype was conducted out in the air using a mixed solvent of dichloromethane and methanol, resulting in a clear brown solution (Fig. S1†). High-quality single crystals were obtained by diffusing ether into the supernatant after centrifuging the raw product (Fig. S2†).

X-ray single-crystal diffraction was initially employed to determine the molecular structure of the $Cu_{47}H_{12}$ NC (Fig. S3†). The cluster crystallized in the $P6_3/m$ space group of the hexagonal crystal system (Table S1†), with each unit cell containing two independent $Cu_{47}H_{12}$ moieties and several dichloromethane solvent molecules (Fig. S4†). The absence of counterions in the lattice indicates that the cluster is electrically neutral. Detailed analysis reveals that the cluster consists of 47 copper atoms, 15 PhSe⁻, 5 PPh₃, and 12 CF₃COO⁻ ligands, resulting in the overall formula of $[Cu_{47}(PhSe)_{15}(PPh_3)_5(CF_3COO)_{12}H_{12}]$ (Fig. 1). It should be noted that the number of hydride atoms in the cluster was determined by mass spectrometry (*vide infra*). The total size of the cluster was measured to be approximately 2.3 nm (Fig. S5†). The overall C_3 symmetry of the cluster is accompanied by a plane perpendicular to the symmetry axis that imparts mirror symmetry to the cluster (Fig. S6†), resulting in only one-sixth of the clusters being present in the asymmetric unit.

The structural anatomy of the Cu_{47} cluster is depicted in Fig. 2. Its core lies a triaugmented triangular prism comprised of 9 copper atoms (Fig. 2a). The Cu_9 polyhedron is referred to as the Johnson solid J_{51}, which is formed by placing a regular tetrahedron on each square face of an equilateral triangular prism, resulting in a convex deltahedron consisting of 14 equilateral triangles. While the framework is frequently observed in rare-earth metal complexes, the identification of a similar structure in coinage metal NCs is uncommon.[58,59] The bond lengths in the Cu_9 unit range from 1.620 to 3.240 Å, with an average value of 2.641 Å (see Table S2† for detailed bond lengths). The average Cu–Cu bond lengths within the Cu_9 kernel are notably shorter than those in previously reported copper NCs, indicating a robust interaction within the kernel.[60] Remarkably, the top shape of the Cu_9 core mirrors the Cu_6 motif found in the previously reported $[Cu_{31}(4\text{-MeO-PhC}\equiv C)_{21}(dppe)_3](ClO_4)_2$ (Cu_{31}, dppe = 1,2-bis(diphenylphosphino)ethane) (Fig. S7†).[49] Surrounding the Cu_9 core are C_3 symmetric Cu_4Se_3 tiles at the top and bottom, flanked by two sets of three Cu_7 and Cu_3Se_3 units along the C_3 axis, forming the $Cu_{38}Se_{15}$ framework (Fig. 2b). The mirror symmetry of the overall structure is reflected in the mirror-symmetric Cu_7 units at the waist and Cu_3Se_3 units at the head of the cluster. It is worth noting that although the subtle difference between Cu_4Se_3 and Cu_3Se_3 units is one copper atom, the Cu–Se bond lengths in the Cu_3Se_3 units are shorter than those in the Cu_4Se_3 units. The Cu–Se bond lengths range from 2.556 Å to 2.518 Å between the central Cu and Se atoms, and from 2.525 Å to 2.495 Å in the periphery. This discrepancy may be attributed to the unique geometry of the Cu_9 core that restricts the growth space of the outer atoms,
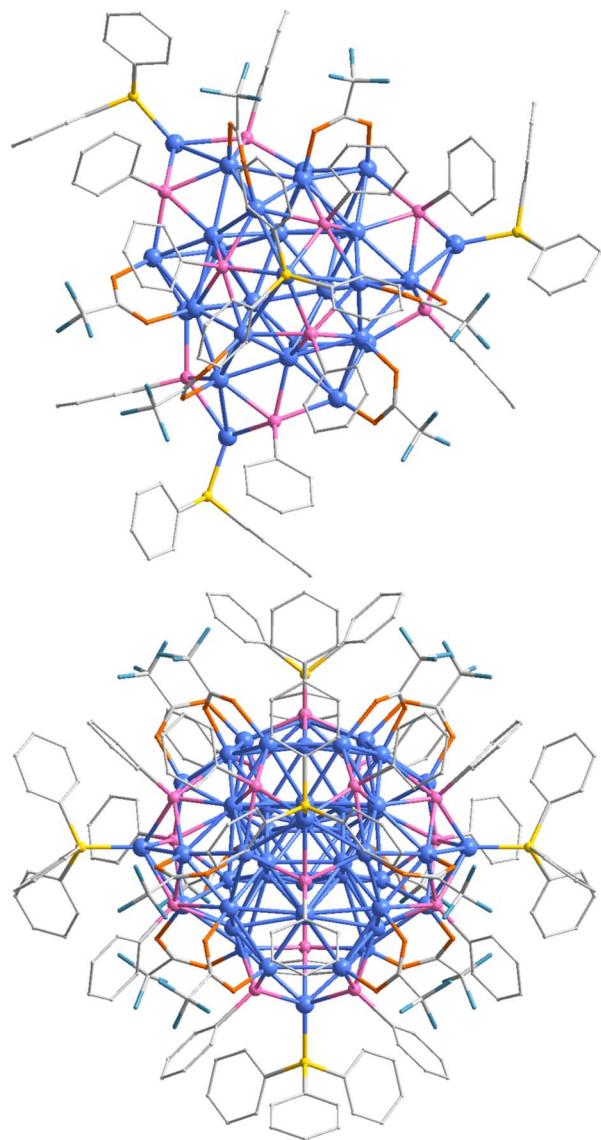
Fig. 1 The structure of the $Cu_{47}H_{12}$ nanocluster in top and side views. Color legend: Cu blue, Se pink, P yellow, O orange, F cyan, and C grey. All H atoms are omitted for clarity.

while the $Cu_{38}Se_{15}$ framework envelops the Cu_9 core akin to a spider web. In the $Cu_{38}Se_{15}$ framework, the average Cu–Cu bond length is 2.675 Å, which is longer than that of the Cu_9 core, suggesting a loose arrangement of Cu atoms in the $Cu_{38}Se_{15}$ framework. From the viewpoint of Se, there are two coordination modes of Se atoms in the clusters: a μ_5 coordination mode at the top and bottom of the overall structure, and a μ_4 coordination at the waist. The Cu–Se bond lengths range from 2.381 Å to 2.675 Å, comparable to those in $[Cu_{23}(PhSe)_{16}(Ph_3P)_8(H)_6]$ BF_4.[61] As shown in Fig. 2c, all phosphine ligands are positioned on symmetry elements (either plane of symmetry or axis of symmetry), collectively forming a double triangular cone shape. The CF_3COO^- ligands adopt the well-known Cu–O–C–O–Cu motifs on the surface of the cluster, arranged in a C_3 symmetry to form a propeller.

2.2 Characterization and electronic structure

As previously mentioned, $Cu_{47}H_{12}$ is proposed to be a neutral cluster, as no counterions were detected in the lattice. To determine the number of hydride atoms and confirm the exact composition of the molecule, mass spectrometry analysis data was obtained in the negative mode. To our satisfaction, a series of distinct peaks in the range of 3500–3900 m/z are observed in the spectrum (Fig. 3a). Upon thorough examination of all potential candidates, the peak that most closely aligns with the target molecule is identified as $[Cu_{47}(PPh_3)_2(CF_3COO)_{11}(PhSe)_{18}H_{12}]^{2-}$. This assignment is substantiated by the excellent correlation observed between the simulated and experimental isotopic patterns (Fig. 3a, inset). Additionally, other peaks can be recognized as fragments originating from the parent clusters (refer to Fig. S8 and S9† for more details). To further validate the presence of hydride atoms in the structure, we synthesized a deuterated analog, designated as $[Cu_{47}(PPh_3)_5(CF_3COO)_{12}(PhSe)_{15}D_{12}]$ (referred to as $Cu_{47}D_{12}$) by using $(PPh_3)_2CuBD_4$ in place of $(PPh_3)_2CuBH_4$ during the cluster synthesis process. The mass spectrum of $Cu_{47}D_{12}$ reveals discernible peaks, the most prominent of which corresponds to $[Cu_{47}(PPh_3)_2(CF_3COO)_{13}(PhSe)_{14}Cl_2(C_4H_{10}O)(CH_3OH)(H_2O)$ $D_{12}]^{2-}$ (Fig. 3b and S10†). The above analysis unequivocally confirms the presence of 12 hydride (deuteride) atoms within the structure.

According to the equation reported by Häkkinen, the number of free valence electrons of $Cu_{47}H_{12}$ is calculated to be 8.[62] It suggests that $Cu_{47}H_{12}$ comprises Cu(0) atoms in its structure. The valence state of copper in the cluster compounds was further investigated utilizing X-ray photoelectron spectroscopy (XPS). In the Cu LMM Auger spectrum (Fig. S11†), the shoulder band observed at 918.5 eV, which is associated with Cu(0) species supports the partial zero oxidation state of copper atoms in $Cu_{47}H_{12}$, while the principal peak at 916.2 eV corresponds to the Cu(I) component. The binding energies for Cu $2p_{3/2}$ and Cu $2p_{1/2}$ are recorded at 932.6 and 952.4 eV, respectively, further suggesting that the Cu atoms in the cluster exist in a state that is intermediate between reduction and oxidation (Fig. S12†). Energy dispersive X-ray spectroscopy corroborated the presence of Se, P, O, F, and C elements in the sample (Fig. S13†). The X-ray powder diffraction (PXRD) pattern of this copper nanocluster aligns with the simulated pattern, indicating that the $Cu_{47}H_{12}$ cluster exhibits good phase purity (Fig. S14†). The proton-decoupled ^{31}P NMR spectrum of $Cu_{47}H_{12}$ in d_6-DMSO is presented in Fig. S15.† The broad singlet peak indicates that the PPh_3 ligands are in a dynamic equilibrium in the solution, at least within the timescale of NMR measurement. From the aforementioned analysis, we conclude that: (1) this cluster represents a rare example of copper-hydride NCs, protected by selenate ligands. The presence of 12 hydrides in the structure endows the cluster with eight free valence electrons, marking it as the first copper hydride NC known to possess up to eight free valence electrons. (2) The involvement of three organic ligands, namely phosphine, selenite, and carboxylate, participated in the passivation of $Cu_{47}H_{12}$ clusters, indicating the potential for customizing the surface and even

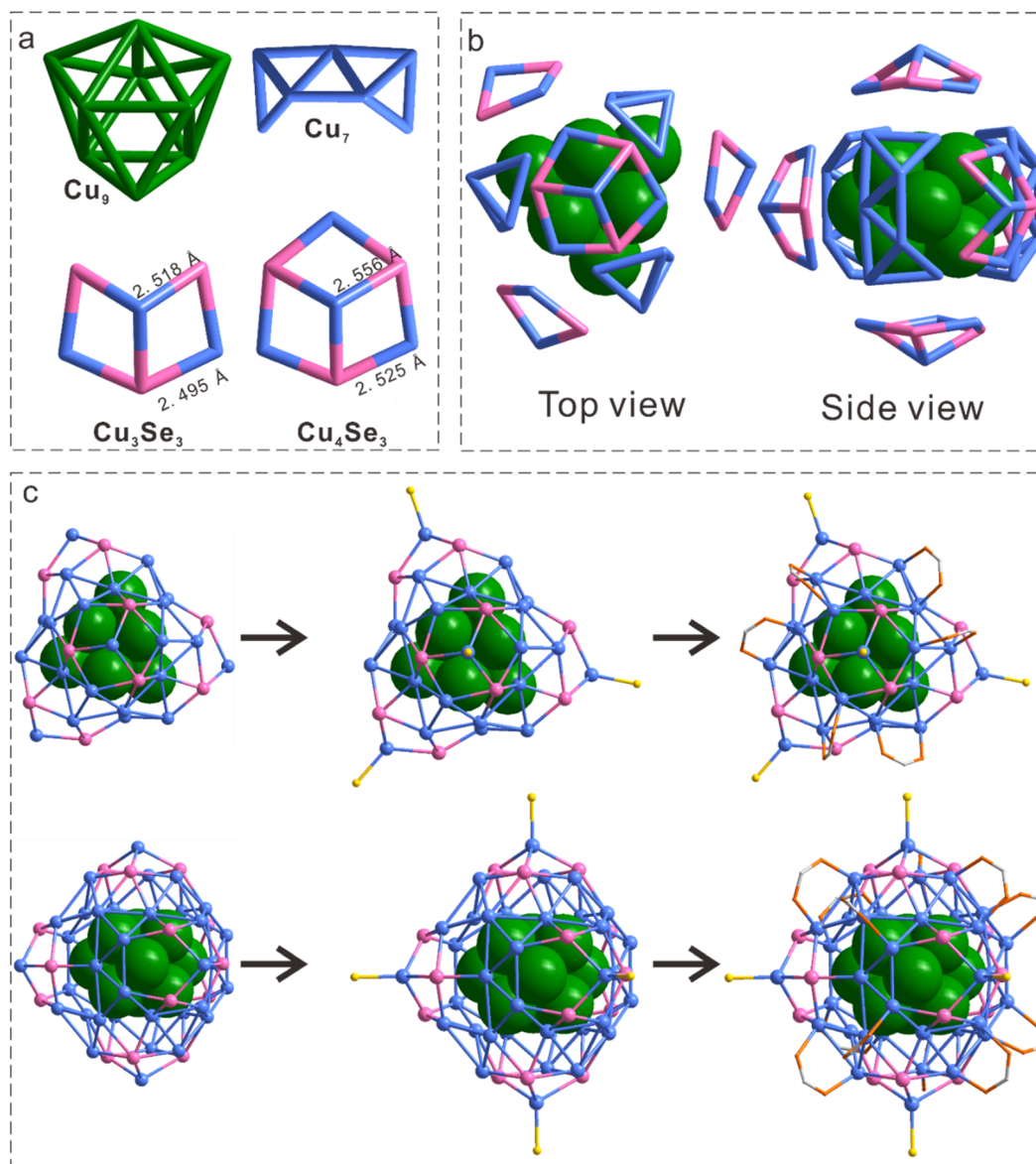Fig. 2 Structural anatomy of the $Cu_{47}H_{12}$ cluster. (a) The Cu_9 kernel, Cu_7, Cu_3Se_3 and Cu_4Se_3 motifs. (b) The top and side view of the assembled structure of the $Cu_9@Cu_{38}Se_{15}$ unit. (c) The top and side view of the $Cu_9@Cu_{38}Se_{15}@P_5@(RCOO)_{12}$ arrangement. Color legend: Cu blue and green, Se pink, P yellow, O orange and C grey. All other atoms are omitted for clarity.

geometric structure of hydride-containing metal NCs through ligand engineering (the related work will be discussed in a subsequent paper).

We endeavored to determine the positions of the hydrides utilizing a multifaceted approach that incorporated various characterization techniques, including mass spectroscopy, nuclear magnetic resonance (NMR), X-ray diffraction, and density functional theory (DFT) computations.[63,64] Fig. S16† shows that the only difference in the ^1H NMR spectra of $Cu_{47}H_{12}$ and $Cu_{47}D_{12}$ reveals a singular distinction at 4.61 ppm, indicating the existence of only one chemical environment for the hydrides in the cluster. Similarly, a solitary peak at 4.43 ppm was observed in the ^2H NMR of $Cu_{47}D_{12}$ in d_6-DMSO, further substantiating the notion of a singular coordination mode for the deuterides (or hydrides) present in the cluster (Fig. S17†).

The proposed positions of the 12 hydrides, which share the same coordination environment, were inferred from the peaks observed in the difference electron density map derived from the crystallographic data (Fig. S18†). The accuracy of the proposed coordinates was corroborated through DFT calculations (*vide infra*). As shown in Fig. S18,† all 12 hydrides exhibit three-fold coordination, forming a triple bridge (or cap) over a triangular arrangement of Cu atoms. The Cu–H distances give an average value of 1.798 Å, which is consistent with the values documented for copper-hydride NCs in the existing literature.[32,37]

To gain deep insight into the electronic properties and rationalize the hydride positions of the title cluster, DFT calculations were then carried out. The electronic structure calculations of the $Cu_{47}H_{12}$ cluster were performed using the
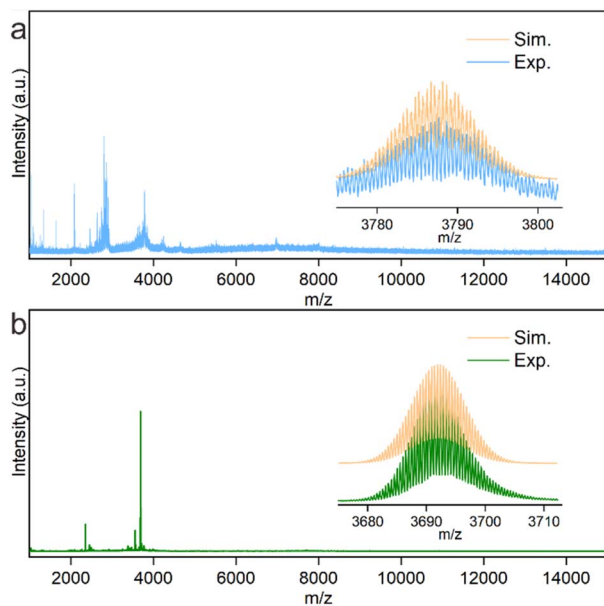
Fig. 3 The ESI-MS spectroscopy of $Cu_{47}H_{12}$ (a) and $Cu_{47}D_{12}$ (b) clusters in the negative mode. Inset is the comparison between the simulated (orange) and experimental (blue and green) isotopic pattern of $[Cu_{47}(PPh_3)_2(CF_3COO)_{11}(PhSe)_{18}H_{12}]^{2-}$ and $[Cu_{47}(PPh_3)_2(CF_3COO)_{13}(PhSe)_{14}Cl_2(C_4H_{10}O)(CH_3OH)(H_2O)D_{12}]^{2-}$.

Vienna Ab initio Simulation Package software. The accuracy of the proposed coordinates was corroborated through DFT calculations. The atomic coordinates of optimized structures of $Cu_{47}H_{12}$ cluster are summarized in Table S3.† Shown in Fig. 4a is the frontier orbital charge densities of the $Cu_{47}H_{12}$ cluster. The analysis reveals the charge density of the lowest unoccupied molecular orbital (LUMO) and the highest occupied molecular orbital (HOMO) orbitals is primarily located near Cu atoms. In the case of $Cu_{47}H_{12}$ cluster, the energy gap between HOMO and LUMO is calculated to be 0.18 eV, suggesting its electronic stability. Fig. 4b displays the total density of states and projected density of states (PDOS) of each element of the $Cu_{47}H_{12}$ cluster. Moreover, the HOMO and LUMO orbitals of the $Cu_{47}H_{12}$ cluster are mainly provided by the Cu elements, which agrees well with the orbital charge densities in Fig. 4a.

2.3 Alloying chemistry and photoluminescence properties

The incorporation of heteroatoms through alloying has emerged as a highly effective approach for tailoring the compositions, structures, electronic structures, and properties of parent metal NCs.[65,66] Although the alloying chemistry of gold and silver NCs has been extensively studied, research concerning the alloying chemistry of copper NCs remains relatively scarce.[67] It is posited that the presence of hydride species in copper-hydride NCs facilitates a distinct alloying chemistry that distinguishes them from their gold and silver NCs. Consequently, the subsequent section investigates the influence of alloying heteroatoms, such as silver, on the parent $Cu_{47}H_{12}$ NCs. From a synthetic perspective, the simultaneous reduction of CF_3COOAg and $Cu(CF_3COO)_2$ under identical reduction
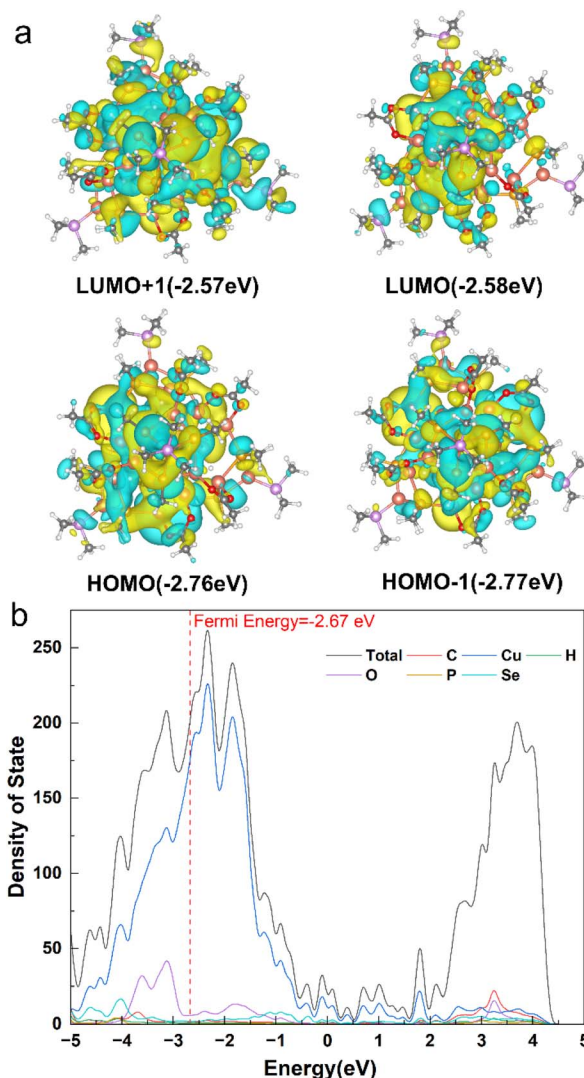

Fig. 4 (a) Frontier orbitals of $Cu_{47}H_{12}$ cluster; (b) the total density of states and projected density of states of $Cu_{47}H_{12}$ cluster. Color legend: Cu bronze, Se lime, P pink, O red, C gray, and H white.

conditions yields dark brown solutions, which exhibit UV-vis spectra that differ slightly different from those of $Cu_{47}H_{12}$ (Fig. S19†).

One might initially assume that akin to the general behaviour observed in gold and silver NCs, alloying would not significantly alter the structures of parent copper NCs. However, the alloying of silver atoms into the $Cu_{47}H_{12}$ framework has a significant effect on its formula and structure, despite maintaining the same number of metal atoms and free valence electrons. Fig. 5a shows that the alloying of silver atoms during the synthesis results in completely different mass spectra. While the $Cu_{47}H_{12}$ cluster is neutral in charge, the newly formed Ag–Cu NCs are positive. The ESI-MS analysis of the alloyed NCs, determined in positive mode, exhibits a series of clear peaks in the range of 2300–2800 m/z (Fig. S20†). These peaks are attributed to the fragments originating from the parental $[(CuAg)_{47}(PhSe)_{18}(PPh_3)_6(CF_3COO)_{12}H_6]^{3+}$ clusters, labelled as
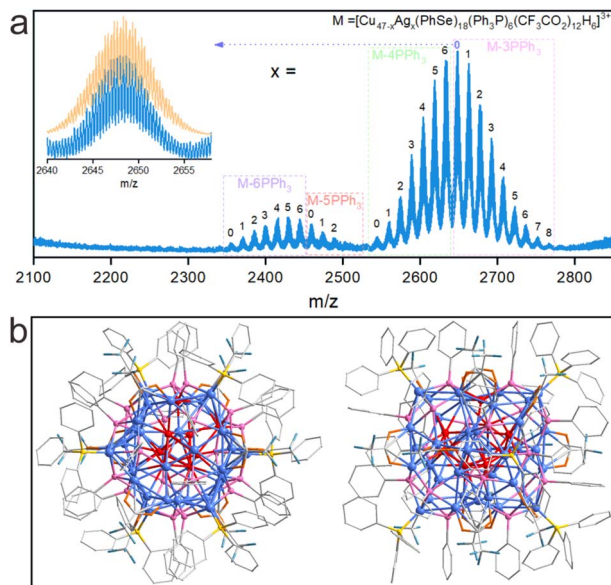
Fig. 5 (a) The ESI-MS spectroscopy of $(CuAg)_{47}H_6$ clusters in the positive mode. Inset is the comparison between the simulated (orange) and experimental (blue) isotopic pattern of $[Cu_{47}(PhSe)_{18}(PPh_3)_3(CF_3COO)_{12}H_6]^{3+}$. (b) Total structure of the $(CuAg)_{47}H_6$ nanocluster in the top and side view. Color legend: Cu blue, Ag red, Se pink, P yellow, O orange, F cyan and C grey. All H atoms are omitted for clarity.

$(CuAg)_{47}H_6$. The observed peak series corresponds to the loss of neutral PPh_3 ligands in quantities of 3, 4, 5, and 6, respectively, from $[(CuAg)_{47}(PhSe)_{18}(PPh_3)_6(CF_3COO)_{12}H_6]^{3+}$ molecules. The assignment is verified by the excellent concordance between the simulated and experimental isotopic patterns. Furthermore, adjacent peaks correspond to species undergoing Ag–Cu exchange, which is consistent with the observed partial occupancy of Ag and Cu in certain positions in the single crystal structure (*vide infra*). It is worth noting that the $(CuAg)_{47}H_6$

clusters also possess eight free valence electrons as well, prompting intriguing inquiries regarding their molecular structure.

High-quality single crystals of $(CuAg)_{47}H_6$ clusters were obtained by a methodology analogous to that employed for $Cu_{47}H_{12}$. In full agreement with the ESI-MS analysis, the tricationic cluster $[Cu_{47}(PhSe)_{18}(PPh_3)_6(CF_3COO)_{12}H_6]^{3+}$, as elucidated through X-ray single crystal diffraction, comprises 47 copper atoms, 18 $PhSe^-$, 6 Ph_3P and 12 CF_3COO^- ligands. As shown in Fig. 5b, the total structure of $(CuAg)_{47}H_6$ is a significant deviation from that of $Cu_{47}H_{12}$. Specifically, the addition of Ag atoms has caused the transformation of the originally regular polyhedral core into a twisted cube-like $Cu_{15}Ag_8$ (Fig. 6a and e). In comparison to the Cu_9 core, the $Cu_{15}Ag_8$ structure presents an average Cu–Cu bond length of 2.762 Å and an average Ag–Cu bond length of 2.784 Å. Furthermore, the motifs surrounding the core have also changed from three to two similar Cu_3Se_3 units (Fig. 6b and f). The number of phosphine ligands in $(CuAg)_{47}H_6$ has increased by one, leading to their different coordination positions from $Cu_{47}H_{12}$ (Fig. 6c and g). Although the quantity of carboxylate ligands remains the same, their spatial arrangement is notably more compact (Fig. 6d and h). The pronounced structural alteration of $(CuAg)_{47}H_6$ relative to $Cu_{47}H_{12}$ is likely attributable to the larger van der Waals atomic radii of Ag in comparison to Cu, which forces the deformation of the parent clusters upon substitution. Importantly, the alloying of silver also engenders obvious modifications in electronic structure and stability. As shown in Fig. S21,† $Cu_{47}H_{12}$ and $(CuAg)_{47}H_6$ display distinct UV-vis absorption peaks. Meanwhile, the ambient decay rates of $(CuAg)_{47}H_6$ in solution were significantly slower than those of $Cu_{47}H_{12}$, which is consistent with previous reports (Fig. S22†).[68] The increased stability of $(CuAg)_{47}H_6$ compared to $Cu_{47}H_{12}$ may be attributed to its larger HOMO–LUMO gap (0.22 eV for $Cu_{47}H_{12}$ and 0.32 eV for $(CuAg)_{47}H_6$, Fig. S23†).

Both $Cu_{47}H_{12}$ and $(CuAg)_{47}H_6$ show luminescent properties. As shown in Fig. 7a, the $Cu_{47}H_{12}$ cluster in *N,N*-
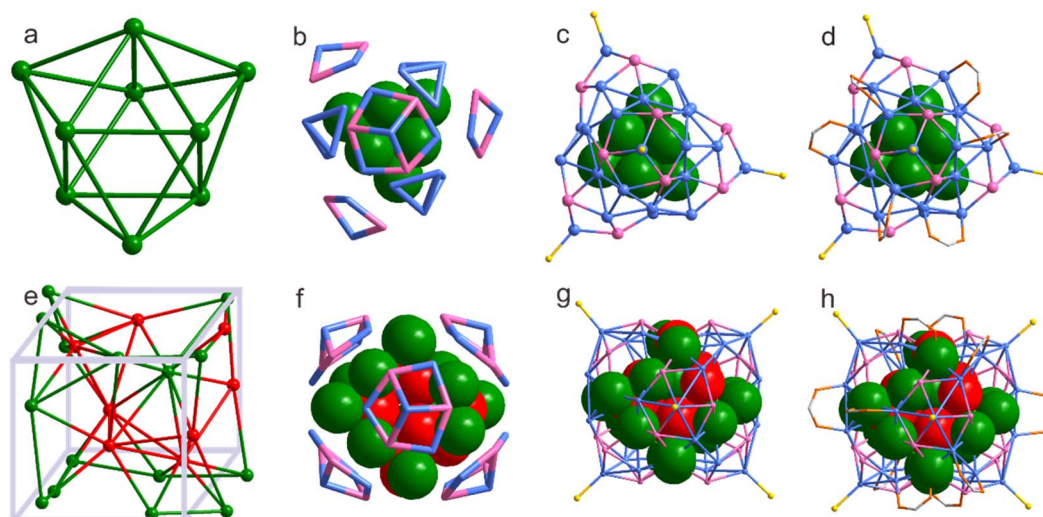

Fig. 6 Structural comparison of $Cu_{47}H_{12}$ (a–d) and $(CuAg)_{47}H_6$ (e–h). Color legend: Cu blue and green, Ag red, Se pink, P yellow, O orange and C grey. All other atoms are omitted for clarity.
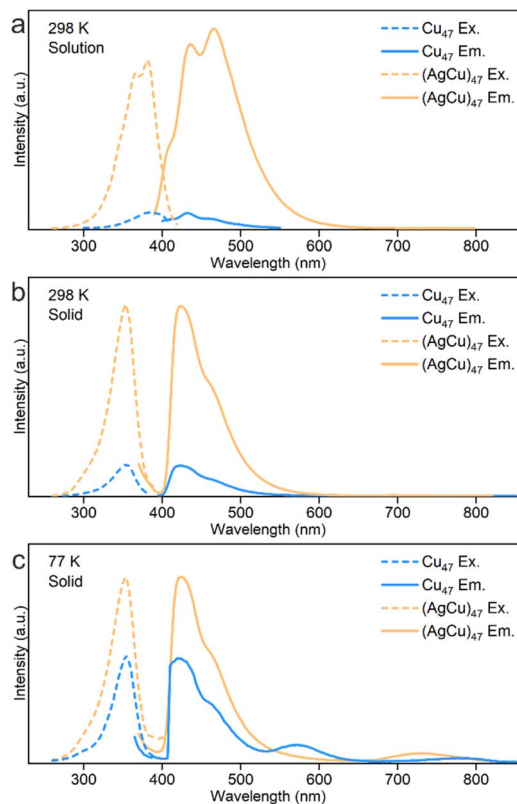
Fig. 7 Excitation and emission spectra of $Cu_{47}H_{12}$ and $(CuAg)_{47}H_6$. (a) DMF solution at 298 K. (b) Solid at 298 K. (c) Solid at 77 K.

dimethylformamide demonstrates dual emission characterized by two peaks at 420 and 463 nm upon excitation at 390 nm. The $(CuAg)_{47}H_6$ also displays a similar emission profile, however, its photoluminescence quantum yield (PLQY) is much lower (2.74% for $Cu_{47}H_{12}$ and 0.31% for $(CuAg)_{47}H_6$). The clusters are expected to emit phosphorescence, as evidenced by their extended photoluminescence lifetimes (exemplified by a lifetime of 7.4840 μs for $Cu_{47}H_{12}$). In their crystalline state, these clusters are also luminescent, displaying blue-shifted emission peaks (Fig. 7b). It is interesting to note that the PLQY of the clusters in their crystalline form is significantly higher than that observed in the solution, for instance, $Cu_{47}H_{12}$ exhibits a PLQY of 2.74% in solution (DMF), while the PLQY in the solid form is measured to be as high as 9.30%. More remarkably, the clusters exhibit triple or even quadruple emission characteristics in the solid state. Upon lowering the temperature from 298 K to 77 K, a new emission peak at 731 nm is observed in the spectrum of $(CuAg)_{47}H_6$. The $Cu_{47}H_{12}$ cluster surprisingly exhibits four peaks (420, 462, 577, and 791 nm) in its emission curves, including one in the near-infrared region. We note that although metal NCs with triple emission properties are infrequently reported in the literature, those exhibiting quadruple-mode emissions have not been reported, to the best of our knowledge.[69,70] It is also worth noting that the intensities of the emission peak at 791 nm for $Cu_{47}H_{12}$ increase significantly as the temperature decreases from 283 K to 83 K, suggesting that

the potential application of this cluster as a molecular luminescent thermometer operating in the NIR region.

3 Conclusions

In conclusion, we present the initial instance of copper nanoclusters doped with hydride, characterized by the presence of eight free valence electrons: $[Cu_{47}(PhSe)_{15}(PPh_3)_5(CF_3COO)_{12}H_{12}]$. The successful isolation, comprehensive characterization, and determination of the structure of this specific cluster have been achieved, unequivocally demonstrating the potential for enhancing the geometric, surface, and electronic properties of metal-hydride nanoclusters in future research endeavors. The alloying chemistry associated with the cluster is relatively novel. The incorporation of silver heteroatoms results in alterations to both composition and structure, giving rise to another new family of eight-electron $[(CuAg)_{47}(PhSe)_{18}(PPh_3)_6(CF_3COO)_{12}H_6]^{3+}$ clusters. Furthermore, these clusters exhibit double, triple, and even quadruple emission properties, which endow them with promising applications in optoelectronics, ratiometric sensing, and biological contexts. This research not only presents the inaugural example of eight-electron copper-hydride nanoclusters, thereby significantly broadening the synthetic, compositional, and structural chemistry of hydride-containing metal nanoclusters but also emphasizes the unique nature of such materials in terms of alloying and photoluminescent properties.

Data availability

The data supporting this article have been included as part of the ESI.†

Author contributions

H. S. conceived and supervised the research project. J. S. synthesized and characterized the samples. W. J. and H. G. investigated the photoluminescence properties under the guide of J. W. S. W. supervised the DFT calculations and analysed the computational results together with J. L. who conducted the calculations. H. S., Z. X., X. T., Z. X. and S. L. were responsible for the data collection and analysis. X. G., D. J., N. Z., and H. S. revised the manuscript.

Conflicts of interest

There are no conflicts to declare.

Acknowledgements

References

1 I. Chakraborty and T. Pradeep, Atomically Precise Clusters of Noble Metals: Emerging Link between Atoms and Nanoparticles, *Chem. Rev.*, 2017, **117**, 8208–8271.

2 R. Jin, C. Zeng, M. Zhou and Y. Chen, Atomically Precise Colloidal Metal Nanoclusters and Nanoparticles: Fundamentals and Opportunities, *Chem. Rev.*, 2016, **116**, 10346–10413.

3 M. Matus and H. Häkkinen, Understanding ligand-protected noble metal nanoclusters at work, *Nat. Rev. Mater.*, 2023, **8**, 372–389.

4 K. Konishi, M. Iwasaki and Y. Shichibu, Phosphine-Ligated Gold Clusters with Core+exo Geometries: Unique Properties and Interactions at the Ligand-Cluster Interface, *Acc. Chem. Res.*, 2018, **51**, 3125–3133.

5 C. Deng, B. Han, Z. Liu, Z. Pan, J. He, Y. Li, Z. Yang, G. Luo, C. Tung, D. Sun and L. Zheng, Hierarchical Homochiral Assembly of Polyhedral Cage-Type Nanoclusters, *CCS Chem.*, 2024, **6**, 2537–2548.

6 B. Han, Z. Liu, L. Feng, Z. Wang, R. Gupta, C. M. Aikens, C. Tung and D. Sun, Polymorphism in Atomically Precise Cu_{23} Nanocluster Incorporating Tetrahedral $[Cu_4]^0$ Kernel, *J. Am. Chem. Soc.*, 2020, **142**, 5834–5841.

7 K. Isozaki, R. Ueno, K. Ishibashi, G. Nakano, H. Z. Yin, K. Iseri, M. Sakamoto, H. Takaya, T. Teranishi and M. Nakamura, Gold Nanocluster Functionalized with Peptide Dendron Thiolates: Acceleration of the Photocatalytic Oxidation of an Amino Alcohol in a Supramolecular Reaction Field, *ACS Catal.*, 2021, **11**, 13180–13187.

8 D. C. Lim, B. Y. Seo, S. G. Nho, D. H. Kim, E. M. Hong, J. Y. Lee, S. Y. Park, C. L. Lee, Y. D. Kim and S. Cho, Emissive Nanoclusters Based on Subnanometer-Sized Au_{38} Cores for Boosting the Performance of Inverted Organic Photovoltaic Cells, *Adv. Energy Mater.*, 2015, **5**, 1500393.

9 S. Li, Z. P. Yan, X. L. Li, Y. J. Kong, H. Y. Li, G. G. Gao, Y. X. Zheng and S. Q. Zang, Stepwise Achievement of Circularly Polarized Luminescence on Atomically Precise Silver Clusters, *Adv. Sci.*, 2020, **7**, 2000738.

10 D. Yang, W. Pei, S. Zhou, J. J. Zhao, W. P. Ding and Y. Zhu, Controllable Conversion of CO_2 on Non-Metallic Gold Clusters, *Angew. Chem., Int. Ed.*, 2020, **59**, 1919–1924.

11 K. Yonesato, S. Yamazoe, D. Yokogawa, K. Yamaguchi and K. Suzuki, A Molecular Hybrid of an Atomically Precise Silver Nanocluster and Polyoxometalates for H_2 Cleavage into Protons and Electrons, *Angew. Chem., Int. Ed.*, 2021, **60**, 16994–16998.

12 Q. You, X. L. Jiang, W. T. Fan, Y. S. Cui, Y. Zhao, S. L. Zhuang, W. M. Gu, L. W. Liao, C. Q. Xu, J. Li and Z. Wu, Pd_8 Nanocluster with Nonmetal-to-Metal- Ring Coordination and Promising Photothermal Conversion Efficiency, *Angew. Chem., Int. Ed.*, 2024, **63**, e202313491.

13 D. Arima and M. Mitsui, Structurally Flexible Au–Cu Alloy Nanoclusters Enabling Efficient Triplet Sensitization and Photon Upconversion, *J. Am. Chem. Soc.*, 2023, **145**, 6994–7004.

14 R. W. Huang, Y. S. Wei, X. Y. Dong, X. Wu, C. X. Du, S. Q. Zang and T. C. W. Mak, Hypersensitive dual-function luminescence switching of a silver-chalcogenolate cluster-based metal–organic framework, *Nat. Chem.*, 2017, **9**, 689–697.

15 J. Chen, P. Gu, G. Ran, Y. Zhang, M. Li, B. Chen, H. Lu, Y. Han, W. Zhang, Z. Tang, Q. Yan, R. Sun, X. Fu, G. Chen, Z. Shi, S. Wang, X. Liu, J. Li, L. Wang, Y. Zhu, J. Shen, B. Z. Tang and C. Fan, Atomically precise photothermal nanomachines, *Nat. Mater.*, 2024, **23**, 271–280.

16 Q. Yao, L. Liu, S. Malola, M. Ge, H. Xu, Z. Wu, T. Chen, Y. Cao, M. F. Matus, A. i. Pihlajamäki, Y. Han, H. Häkkinen and J. Xie, Supercrystal engineering of atomically precise gold nanoparticles promoted by surface dynamics, *Nat. Chem.*, 2023, **15**, 230–239.

17 P. Chandrashekar, G. Sardar, T. Sengupta, A. C. Reber, P. K. Mondal, D. Kabra, S. N. Khanna, P. Deria and S. Mandal, Modulation of Singlet-Triplet Gap in Atomically Precise Silver Cluster-Assembled Material, *Angew. Chem., Int. Ed.*, 2024, **63**, e202317345.

18 C. Zhang, Z. Wang, W. Si, H. Chu, L. Zhou, T. Li, X. Huang, Z. Gao, M. Azam, C. Tung, P. Cui and D. Sun, Dynamic and transformable Cu_{12} cluster-based C-H···π-stacked porous supramolecular frameworks, *Nat. Commun.*, 2023, **14**, 6413.

19 Q. Wu, D. Si, P. Sun, Y. Dong, S. Zheng, Q. Chen, S. Ye, D. Sun, R. Cao and Y. Huang, Atomically Precise Copper Nanoclusters for Highly Efficient Electroreduction of CO_2 towards Hydrocarbons *via* Breaking the Coordination Symmetry of Cu Site, *Angew. Chem., Int. Ed.*, 2023, **62**, e202306822.

20 A. J. Jordan, G. Lalic and J. P. Sadighi, Coinage Metal Hydrides: Synthesis, Characterization, and Reactivity, *Chem. Rev.*, 2016, **116**, 8318–8372.

21 C. Sun, B. K. Teo, C. Deng, J. Lin, G. Luo, C. H. Tung and D. Sun, Hydrido-coinage-metal clusters: rational design, synthetic protocols and structural characteristics, *Coord. Chem. Rev.*, 2021, **427**, 213576.

22 A. Baghdasaryan and T. Bürgi, Copper nanoclusters: designed synthesis, structural diversity, and multiplatform applications, *Nanoscale*, 2021, **13**, 6283–6340.

23 G. Luo, Z. Pan, B. Han, G. Dong, C. Deng, M. Azam, Y. Tao, J. He, C. Sun and D. Sun, Total Structure, Electronic Structure and Catalytic Hydrogenation Activity of Metal-Deficient Chiral Polyhydride Cu_{57} Nanoclusters, *Angew. Chem., Int. Ed.*, 2023, **62**, e202306849.

24 H. Yi, S. M. Han, S. Song, M. Kim, E. Sim and D. Lee, Superatom-in-Superatom $[RhH@Ag_{24}(SPhMe_2)_{18}]^{2-}$ Nanocluster, *Angew. Chem., Int. Ed.*, 2021, **60**, 22293–22300.

25 M. Girod, M. Krstić, R. Antoine, L. MacAleese, J. Lemoine, A. Zavras, G. N. Khairallah, V. Bonačić-Koutecký, P. Dugourd and R. A. J. O'Hair, Formation and Characterisation of the Silver Hydride Nanocluster Cation

$[Ag_3H_2((Ph_2P)_2CH_2)]^+$ and Its Release of Hydrogen, *Chem.–Eur. J.*, 2014, **20**, 16626–16633.

26 T. H. Chiu, J. H. Liao, Y. Y. Wu, J. Y. Chen, Y. J. Chen, X. P. Wang, S. Kahlal, J. Y. Saillard and C. W. Liu, Hydride Doping Effects on the Structure and Properties of Eight-Electron Rh/Ag Superatoms: The $[RhH_x@Ag_{21}-x\{S_2P(O^nPr)_2\}_{12}]$ $(x = 0-2)$ Series, *J. Am. Chem. Soc.*, 2023, **145**, 16739–16747.

27 L. Gao, K. C. Wei, T. Wu, J. Dong, D. Jiang, S. H. Sun and L. S. Wang, A Heteroleptic Gold Hydride Nanocluster for Efficient and Selective Electrocatalytic Reduction of CO_2 to CO, *J. Am. Chem. Soc.*, 2022, **144**, 5258–5262.

28 Q. Tang, Y. Lee, D. Y. Li, W. Choi, C. W. Liu, D. Lee and D. Jiang, Lattice-Hydride Mechanism in Electrocatalytic CO_2 Reduction by Structurally Precise Copper-Hydride Nanoclusters, *J. Am. Chem. Soc.*, 2017, **139**, 9728–9736.

29 C. Sun, N. Mammen, S. Kaappa, P. Yuan, G. Deng, C. Zhao, J. Yan, S. Malola, K. Honkala, H. Hakkinen, B. K. Teo and N. F. Zheng, Atomically Precise, Thiolated Copper-Hydride Nanoclusters as Single-Site Hydrogenation Catalysts for Ketones in Mild Conditions, *ACS Nano*, 2019, **13**, 5975–5986.

30 A. J. Edwards, R. S. Dhayal, P. K. Liao, J. H. Liao, M. H. Chiang, R. O. Piltz, S. Kahlal, J. Y. Saillard and C. W. Liu, Chinese puzzle molecule: a 15 hydride, 28 copper atom nanoball, *Angew. Chem., Int. Ed.*, 2014, **53**, 7214–7218.

31 S. Lee, M. S. Bootharaju, G. Deng, S. Malola, W. Baek, H. Hakkinen, N. F. Zheng and T. Hyeon, $[Cu_{32}(PET)_{24}H_8Cl_2](PPh_4)_2$: A Copper Hydride Nanocluster with a Bisquare Antiprismatic Core, *J. Am. Chem. Soc.*, 2020, **142**, 13974–13981.

32 R. P. Brocha Silalahi, Y. Jo, J. Liao, T. Chiu, E. Park, W. Choi, H. Liang, S. Kahlal, J. Saillard, D. Lee and C. W. Liu, Hydride-containing 2-Electron Pd/Cu Superatoms as Catalysts for Efficient Electrochemical Hydrogen Evolution, *Angew. Chem., Int. Ed.*, 2023, **62**, e202301272.

33 T. Chiu, J. Liao, F. Gam, Y. Wu, X. Wang, S. Kahlal, J. Saillard and C. W. Liu, Hydride-Containing Eight-Electron Pt/Ag Superatoms: Structure, Bonding, and Multi-NMR Studies, *J. Am. Chem. Soc.*, 2022, **144**, 10599–10607.

34 L. Tang, Y. Luo, X. Ma, B. Wang, M. Ding, R. Wang, P. Wang, Y. Pei and S. Wang, Poly-Hydride $[AuI_7(PPh_3)_7H_5](SbF_6)_2$ cluster complex: Structure, Transformation, and Electrocatalytic CO_2 Reduction Properties, *Angew. Chem., Int. Ed.*, 2023, **62**, e202300553.

35 R. S. Dhayal, J. H. Liao, S. Kahlal, X. Wang, Y. C. Liu, M. H. Chiang, W. E. van Zyl, J. Y. Saillard and C. W. Liu, $[Cu_{32}(H)_{20}\{S_2P(O^iPr)_2\}_{12}]$: The Largest Number of Hydrides Recorded in a Molecular Nanocluster by Neutron Diffraction, *Chem.–Eur. J.*, 2015, **21**, 8369–8674.

36 R. S. Dhayal, J. H. Liao, X. Wang, Y. C. Liu, M. H. Chiang, S. Kahlal, J. Y. Saillard and C. W. Liu, Diselenophosphate-Induced Conversion of an Achiral $[Cu_{20}H_{11}\{S_2P(O^iPr)_2\}_9]$ into a Chiral $[Cu_{20}H_{11}\{Se_2P(O^iPr)_2\}_9]$ Polyhydrido Nanocluster, *Angew. Chem., Int. Ed.*, 2015, **54**, 13604–13608.

37 K. K. Chakrahari, R. P. B. Silalahi, T. Chiu, X. Wang, N. Azrou, S. Kahlal, Y. Liu, M. Chiang, J. Saillard and

38 S. Maity, S. Takano, S. Masuda and T. Tsukuda, Bonding and Electronic Interactions of Hydrogen with Gold Superatoms, *J. Phys. Chem. C*, 2024, **128**, 19–30.

39 S. Takano, H. Hirai, S. Muramatsu and T. Tsukuda, Hydride-Doped Gold Superatom $(Au_9H)^{2+}$: Synthesis, Structure, and Transformation, *J. Am. Chem. Soc.*, 2018, **140**, 8380–8383.

40 S. Takano, H. Hirai, S. Muramatsu and T. Tsukuda, Hydride-Mediated Controlled Growth of a Bimetallic $(Pd@Au_8)^{2+}$ Superatom to a Hydride-Doped $(HPd@Au_{10})^{3+}$ Superatom, *J. Am. Chem. Soc.*, 2018, **140**, 12314–12317.

41 J. Dong, J. R. Robinson, Z. Gao and L. Wang, Selective Semihydrogenation of Polarized Alkynes by a Gold Hydride Nanocluster, *J. Am. Chem. Soc.*, 2022, **144**, 12501–12509.

42 V. K. Kulkarni, B. N. Khiarak, S. Takano, S. Malola, E. L. Albright, T. I. Levchenko, M. D. Aloisio, C. T. Dinh, T. Tsukuda, H. Häkkinen and C. M. Crudden, N-Heterocyclic Carbene-Stabilized Hydrido Au_{24} Nanoclusters: Synthesis, Structure, and Electrocatalytic Reduction of CO_2, *J. Am. Chem. Soc.*, 2022, **144**, 9000–9006.

43 R. S. Dhayal, W. E. van Zyl and C. W. Liu, Polyhydrido Copper Clusters: Synthetic Advances, Structural Diversity, and Nanocluster-to-Nanoparticle Conversion, *Acc. Chem. Res.*, 2016, **49**, 86–95.

44 R. W. Huang, J. Yin, C. Dong, A. Ghosh, M. J. Alhilaly, X. Dong, M. N. Hedhili, E. Abou-Hamad, B. Alamer, S. Nematulloev, Y. Han, O. F. Mohammed and O. M. Bakr, $[Cu_{81}(PhS)_{46}(^tBuNH_2)_{10}(H)_{32}]^{3+}$ Reveals the Coexistence of Large Planar Cores and Hemispherical Shells in High-Nuclearity Copper Nanoclusters, *J. Am. Chem. Soc.*, 2020, **142**, 8696–8705.

45 K. Chakrahari, J. Liao, R. P. B. Silalahi, T. Chiu, J. Liao, X. Wang, S. Kahlal, J. Saillard and C. W. Liu, Isolation and Structural Elucidation of 15-Nuclear Copper Dihydride Clusters: An Intermediate in the Formation of a Two-Electron Copper Superatom, *Small*, 2021, **17**, 2002544.

46 R. P. Brocha Silalahi, H. Liang, Y. Jo, J. Liao, T. Chiu, Y. Wu, X. Wang, S. Kahlal, Q. Wang, W. Choi, D. Lee, J. Saillard and C. W. Liu, Hydride-Containing Pt-doped Cu-rich Nanoclusters: Synthesis, Structure, and Electrocatalytic Hydrogen Evolution, *Chem. Eur. J.*, 2024, **30**, e202303755.

47 T. D. Nguyen, Z. R. Jones, B. R. Goldsmith, W. R. Buratto, G. Wu, S. L. Scott and T. W. Hayton, A Cu_{25} Nanocluster with Partial Cu(0) Character, *J. Am. Chem. Soc.*, 2015, **137**, 13319–13324.

48 A. Chen, X. Kang, S. Jin, W. Du, S. Wang and M. Zhu, Gram-Scale Preparation of Stable Hydride M@Cu_{24} (M = Au/Cu) Nanoclusters, *J. Phys. Chem. Lett.*, 2019, **10**, 6124–6128.

49 T. Jia, Z. J. Guan, C. Zhang, X. Z. Zhu, Y. X. Chen, Q. Zhang, Y. Yang and D. Sun, Eight-Electron Superatomic Cu_{31} Nanocluster with Chiral Kernel and NIR-II Emission, *J. Am. Chem. Soc.*, 2023, **145**, 10355–10363.

50 M. Qu, F. Q. Zhang, D. H. Wang, H. Li, J. J. Hou and X. M. Zhang, Observation of Non-FCC Copper in Alkynyl-

Protected Cu$_{53}$ Nanoclusters, *Angew. Chem., Int. Ed.*, 2020, **59**, 6507–6512.

51 Y. Zhong, J. Liao, T. Chiu, Y. Wu, S. Kahlal, M. J. McGlinchey, J. Saillard and C. W. Liu, Intercluster exchanges leading to hydride-centered bimetallic clusters: a multi-NMR, X-ray crystallographic, and DFT study, *Dalton Trans.*, 2021, **50**, 4727–4734.

52 S. Sharma, K. K. Chakrahari, J. Saillard and C. W. Liu, Structurally Precise Dichalcogenolate-Protected Copper and Silver Superatomic Nanoclusters and Their Alloys, *Acc. Chem. Res.*, 2018, **51**, 2475–2483.

53 Z. Qin, S. Sharma, C. Wan, S. Malola, W. Xu, H. Häkkinen and G. Li, A Homoleptic Alkynyl-Ligated [Au$_{13}$Ag$_{16}$L$_{24}$]$^{3-}$ Cluster as a Catalytically Active Eight-Electron Superatom, *Angew. Chem., Int. Ed.*, 2021, **60**, 970–975.

54 H. Shen, L. Wang, O. López-Estrada, C. Hu, Q. Wu, D. Cao, S. Malola, B. K. Teo, H. Häkkinen and N. F. Zheng, Copper-hydride nanoclusters with enhanced stability by N-heterocyclic carbenes, *Nano Res.*, 2021, **14**, 3303–3308.

55 Q. Xu, X. Gong, Z. Zhao, L. Wang, J. Sun, J. He, S. Li and H. Shen, Comprehensive and practical guidelines for reduction synthesis of atomically precise coinage–metal nanoclusters, *Polyoxometalates*, 2025, **4**, 9140075.

56 J. Sun, X. K. Tang, Z. H. Liu, Z. L. Xie, B. Z. Yan, R. F. Yin, C. Chaolumen, J. Zhang, W. H. Fang, J. Y. Wei and H. Shen, Labile Ligands Protected Cu$_{50}$ Nanoclusters with Tailorable Optical Limiting Effect, *ACS mater. lett.*, 2024, **6**, 281–289.

57 Y. Gao, X. Sun, X. Tang, X. Zie, G. Tian, Z. Nan, H. Yang and H. Shen, An alkynyl-protected Ag$_{13-x}$Cu$_{6+x}$ nanocluster for catalytic hydrogenation, *Dalton Trans.*, 2023, **52**, 52–57.

58 W. Gong, H. Arman, Z. Chen, Y. Xie, F. A. Son, H. Cui, X. Chen, Y. Shi, Y. Liu, B. Chen, O. K. Farha and Y. Cui, Highly Specific Coordination-Driven Self-Assembly of 2D Heterometallic Metal–Organic Frameworks with Unprecedented Johnson-type (J$_{51}$) Nonanuclear Zr-Oxocarboxylate Clusters, *J. Am. Chem. Soc.*, 2021, **143**, 657–663.

59 R. J. Frick, A. B. Pribil, T. S. Hofer, B. R. Randolf, A. Bhattacharjee and B. M. Rode, Structure and Dynamics of the U^{4+} Ion in Aqueous Solution: An *ab Initio* Quantum Mechanical Charge Field Molecular Dynamics Study, *Inorg. Chem.*, 2009, **48**, 3993–4002.

60 S. Biswas, A. Pal, M. K. Jena, S. Hossain, J. Sakai, S. Das, B. Sahoo, B. Pathak and Y. Negishi, Luminescent Hydride-Free [Cu$_7$(SC$_5$H$_9$)$_7$(PPh$_3$)$_3$] Nanocluster: Facilitating Highly Selective C–C Bond Formation, *J. Am. Chem. Soc.*, 2024, **146**, 20937–20944.

61 R. W. Huang, J. Yin, C. Dong, P. Maity, M. N. Hedhili, S. Nematulloev, B. Alamer, A. Ghosh, O. F. Mohammed and O. M. Bakr, [Cu$_{23}$(PhSe)$_{16}$(Ph$_3$P)$_8$(H)$_6$]·BF$_4$: Atomic-Level Insights into Cuboidal Polyhydrido Copper Nanoclusters and Their Quasi-simple Cubic Self-Assembly, *ACS Mater. Lett.*, 2021, **3**, 90–99.

62 H. Häkkinen, Atomic and electronic structure of gold clusters: understanding flakes, cages and superatoms from simple concepts, *Chem. Soc. Rev.*, 2008, **37**, 1847–1859.

63 X. Yuan, C. Sun, X. Li, S. Malola, B. K. Teo, H. Hakkinen, L. S. Zheng and N. F. Zheng, Combinatorial Identification of Hydrides in a Ligated Ag$_{40}$ Nanocluster with Noncompact Metal Core, *J. Am. Chem. Soc.*, 2019, **141**, 11905–11911.

64 J. Liao, R. P. Brocha Silalahi, T. Chiu and C. W. Liu, Locating Interstitial Hydrides in MH$_2$@Cu$_{14}$ (M = Cu, Ag) Clusters by Single-Crystal X-ray Diffraction, *ACS Omega*, 2023, **8**, 31541–31547.

65 X. Liu, E. Wang, M. Zhou, Y. Wan, Y. Zhang, H. Liu, Y. Zhao, J. Li, Y. Gao and Y. Zhu, Asymmetrically Doping a Platinum Atom into a Au$_{38}$ Nanocluster for Changing the Electron Configuration and Reactivity in Electrocatalysis, *Angew. Chem., Int. Ed.*, 2022, **61**, e202207685.

66 A. Ghosh, O. F. Mohammed and O. M. Bakr, Atomic-Level Doping of Metal Clusters, *Acc. Chem. Res.*, 2018, **51**, 3094–3103.

67 X. Kang, Y. Li, M. Zhu and R. Jin, Atomically precise alloy nanoclusters: syntheses, structures, and properties, *Chem. Soc. Rev.*, 2020, **49**, 6443–6514.

68 D. Zhang, P. Pan, X. Du, X. Kang and M. Zhu, Rethinking the stability of metal nanoclusters: the individual *versus* the collective, *Nanoscale*, 2024, **16**, 11513–11517.

69 W. Si, C. Zhang, M. Zhou, W. Tian, Z. Wang, Q. Hu, K. Song, L. Feng, X. Huang, Z. Gao, C. H. Tung and D. Sun, Two triplet emitting states in one emitter: Near-infrared dual-phosphorescent Au$_{20}$ nanocluster, *Sci. Adv.*, 2023, **9**, eadg3587.

70 Q. Li, D. Zhou, J. Chai, W. Y. So, T. Cai, M. Li, L. A. Peteanu, O. Chen, M. Cotlet, X. Wendy Gu, H. Zhu and R. Jin, Structural distortion and electron redistribution in dual-emitting gold nanoclusters, *Nat. Commun.*, 2020, **11**, 2897.